Research Article Vol. 31, No. 5 / 27 Feb 2023 / Optics Express 8049
Optics EXPRESS

Freeform reflector light source used for space traceable spectral radiance calibration on the solar reflected band

YE JIANG,[1,2] JIEWEN TIAN,[3] WEI FANG,[1] DENGHUI HU,[4] AND XIN YE[1,*]

[1]Changchun Institute of Optics, Fine Mechanics and Physics, Chinese Academy of Sciences, Changchun 130033, China
[2]University of Chinese Academy of Sciences, Beijing 100049, China
[3]The Northern Institute of Electronic Equipment of China, Beijing 100191, China
[4]Innovation Academy for Microsatellites of Chinese Academy of Science, Shanghai 200120, China
[*]yexin@ciomp.ac.cn

Abstract: For purpose of improving the accuracy of in-orbit radiometric calibration of Chinese Space-based Radiometric Benchmark (CSRB) reference payload on the reflected solar band and reduce resource consumption, this paper proposed a freeform reflector radiometric calibration light source system based on the beam shaping characteristics of the freeform surface. The design method of initial structure discretization based on Chebyshev points was used to design and solve the freeform surface, and the feasibility of the design method was verified by optical simulation. The designed freeform surface is machined and tested, and the test results show that the surface roughness root mean square (RMS) of the freeform reflector is 0.61 μm, which indicates that the continuity of the machined surface is good. The optical characteristics of the calibration light source system are measured, the results show that the irradiance uniformity and radiance uniformity are better than 98% in the effective illumination area of 100 mm × 100 mm on the target plane. The constructed freeform reflector calibration light source system can meet the requirements of large area, high uniformity and light weight for onboard calibration of the payload of the radiometric benchmark, improving the measurement accuracy of spectral radiance on the reflected solar band.

1. Introduction

Radiation calibration is an important step in the development of space optical remote sensing load and an important prerequisite for obtaining high-quality remote sensing data [1]. The calibration light source is an important part of the onboard radiometric calibration system, which determines the consumption of space, load, energy, and other resources by the whole calibration system to a large extent. At the same time, the characteristics of the target light source also directly limit the accuracy of radiation calibration. At present, there are still some problems in the radiometric calibration of space remote sensors, such as the inconsistency of radiometric calibration values between different remote sensors, the incomparability of data and the low accuracy of the radiometric calibration [2]. To this end, China put forward the concept of a space radiation measurement reference satellite in 2006 and launched the Chinese Space-based Radiometric Benchmark (CSRB) project [3,4]. The purpose of the project is to launch a radiation reference satellite with self-calibration capability, use a new in-orbit calibration system to cross-calibrate the in-orbit satellite, establish a high-precision space radiation reference, and unify the onboard radiation scale, which coincides with the Traceable Radiometry Underpinning Terrestrial-and Helio-Studies (TRUTHS) and the Climate Absolute Radiance and Refractivity

#481105 https://doi.org/10.1364/OE.481105
Journal © 2023 Received 21 Nov 2022; revised 21 Jan 2023; accepted 23 Jan 2023; published 17 Feb 2023

Optics EXPRESS

Observatory (CLARREO) projects proposed by the National Physical Laboratory (NPL) and National Aeronautics and Space Administration (NASA) respectively [5,6].

Under the support of CSRB, Changchun Institute of Optics, Fine Mechanics and Physics (CIOMP), Chinese Academy of Sciences proposed an onboard radiometric calibration scheme [7], which is traceable to the Space Cryogenic Absolute Radiometer (SCAR) [8], the purpose is to establish an onboard radiance benchmark with an uncertainty of better than 1% on the reflected solar band. The calibration system transfers the reference of SCAR to a Transmitted Radiometer (TR) that can measure both radiant power and radiance [9]. And then the TR and the Earth-Moon Imaging Spectrometer (EMIS) simultaneously observe the calibration light source to complete the full-field and full-aperture radiation calibration. The primary role of the TR is to convert from the spectral power responsivity traceable to the SCAR to the spectral radiance responsivity and transfer it to the EMIS (the detailed traceability chain will be described in section 2.1). In the calibration process, the target light source needs to fill the field of view and aperture of the EMIS and TR, and therefore its size needs to be large enough. At the same time, due to the mismatch between the observation area of the EMIS and TR, to achieve higher calibration accuracy, a very strict requirement is put forward for the uniformity of the whole spectral calibration light source. The existing onboard calibration light source system on reflected solar band usually takes the sunlight or halogen tungsten lamp as the light source and uses the integrating sphere or diffuser to homogenize the light to form a uniform target light source [10–13]. When the diffuser is used to homogenize the light, the intensity and stability of the light will change with the change of the incident light field angle, which is easy to introduce the response error of the detector caused by the uneven incident angle and position of the incident light. Using the integrating sphere to homogenize light can achieve high uniformity, but to cover the aperture of EMIS, the volume and weight of the integrating sphere will be very large, which will be a huge consumption of onboard resources. In addition, the off-axis parabolic mirror can obtain a large area extended light source, but the optical path deflection and collimation will require multiple mirrors, which will undoubtedly increase the complexity of the calibration system structure and cannot meet the uniformity requirements. Therefore, due to the current situation that the onboard lighting system cannot take into account both large area, high uniformity and simple structure, we urgently need a new onboard calibration light source system to meet the requirement of radiation calibration accuracy of the reference satellite.

With the development of freeform surfaces, the lighting output enters the era of “custom”. The system precisely controls the light direction to reach the predetermined area, and the design freedom is high [14–16]. This not only makes the spatial layout of the optical system more flexible but also improves the energy utilization efficiency and simplifies the lighting system structure. In addition, the size and uniformity of the outgoing spot of the freeform can be accurately controlled by a reasonable surface design. The beam shaping ability of freeform surface brings a new idea for the design of the onboard whole spectral calibration light source system, which enables us to obtain large-size and high-uniformity target light source by using a single freeform surface.

In this paper, a direct discretization method of a freeform surface is proposed based on existing design methods, and the design, simulation and analysis of the freeform reflector of the SCAR-based calibration system are presented. Combining the homogenization ability of the integrating sphere and diffuser and the beam shaping ability of the freeform reflector, a new onboard calibration light source system is constructed. The system not only takes the energy, load and space utilization onboard into account but also provides a large size calibration light source with ultra-high uniformity. The rest of this paper is organized as follows. In Section 2, we introduce the design concept of the calibration light source system and the freeform reflector and present the design requirements of the light source system in combination with the SCAR-based calibration scheme. In Section 3, we propose the design and solving method of the freeform

Optics EXPRESS

surface. In Section 4, we design, simulate, manufactured and test the freeform calibration light source system in detail. In Sections 5 and 6, we give the discussion and conclusion respectively.

2. Design concept

2.1. Freeform calibration light source system design concept

The light path of the whole spectral calibration light source (composed of halogen tungsten lamp integrating sphere, freeform reflector and diffuser) of the SCAR-based radiation calibration system is shown by the bold arrow in Fig. 1. The freeform calibration light source system adopts an off-axis reflection lighting scheme, which avoids the influence of color difference introduced by the transmission scheme on calibration. We effectively combined the homogenizing light ability of the integrating sphere and the diffuser with the beam shaping ability of the freeform surface, a small diameter integrating sphere with a halogen tungsten lamp is used to vertically illuminate the diffuser by the freeform reflector as the whole spectral calibration light source. The single-mirror lighting method can shorten the optical path effectively and simplify the optical path structure to the greatest extent. The small-diameter integrating sphere can output stronger spectral radiance with a low-power halogen tungsten lamp, which greatly improves the energy utilization rate of the light source system. The off-axis reflection lighting path avoids all the components in the calibration system, making the entire on-board layout very compact and reducing the reflection of light in the system. Therefore, this scheme not only reduces the impact of stray light on the calibration accuracy, but also improves the space utilization of the SCAR-based radiation calibration system.

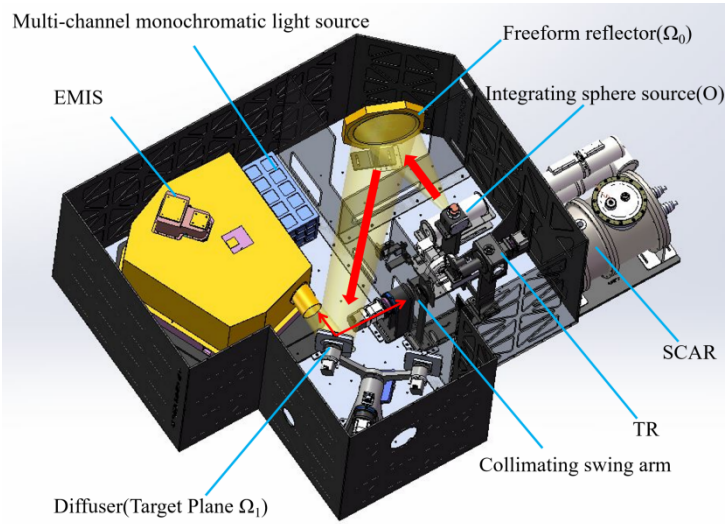

Fig. 1. Light path of the whole spectral calibration light source system of SCAR-based radiation calibration.

As shown in Fig. 1, a multi-channel monochromatic light source was used to achieve the multi-spectral power calibration of the Transfer Radiometer (TR) traced to SCAR. The multi-channel monochromatic light source is connected via fibers to a collimating swing arm, which can introduce the monochromatic light into TR and SCAR in turn (the fibers are not shown in Fig. 1). The TR is used to achieve high-precision conversion and measurement from power to radiance, and establish secondary reference. The uncertainty of radiance measurement is better than 0.55% [9]. The multi-spectral radiance of the whole spectral light source can be calibrated by the TR. Since the spectral curve of the halogen tungsten lamp in the whole spectral

Optics EXPRESS

light source is smooth without mutation, the secondary reference can be converted into the hyperspectral radiance reference by hyperspectral curve reconstruction. As shown by the thin arrow in Fig. 1, TR and hyperspectral imaging system, the Earth-Moon Imaging Spectrometer (EMIS), simultaneously observe the diffuser to achieve high precision radiometric calibration on the reflected solar band. The placement of the diffuser ensures that EMIS and TR can observe the diffuser in a symmetric direction of ±45°, which minimizes the difference between the reflectance of the diffuser at different angles. However, because the observation area of EMIS and TR on the diffuser are different, the irradiance of the reflected light from the freeform reflector to the diffuser is supposed to very uniform to ensure higher radiation value transfer accuracy. The size of the diffuser is 120 mm × 120 mm. EMIS and TR have a maximum observation area of 90 mm on the diffuser, so 100 mm × 100 mm is sufficient to cover their aperture and field of view. After analysis, the radiance uniformity is supposed to be better than 98% in the effective illumination area of 100 mm × 100 mm. The radiance uniformity of the diffuser is affected by the uniformity of its reflectance and the uniformity of the irradiance of the incident light. The diffuser we used is of very good reflectance uniformity, so we want the irradiance uniformity of the incident light of the diffuser, that is, the reflected light of the freeform reflector to be also better than 98%.

2.2. Freeform reflector design concept

Many ideas have been put forward for the construction and solution of freeform surface. However, the current freeform surface design methods are difficult to form a smooth and continuous freeform reflector that can be used for onboard calibration light source system and generate large area uniform light spots. Schruben [17] constructed an illumination system based on mathematical principles and obtained the mathematical model of the elliptic MA (Monge-Ampère) equation of the asymmetric freeform reflector illumination system. But the partial differential equation has high nonlinearity, making its solution very complicated [18,19]. Oliker et al. [20,21] proposed the supported cone method, which is based on illumination discretization. Simultaneous Multiple Surface (SMS) is used to construct the freeform surface by concatenating multiple surfaces, but this makes the resulting surface shape not smooth and continuous. Wu et al. [22–24] solved the elliptic MA equation of freeform reflector by using the Newton descent method and obtained a continuous smooth surface model. However, this method only applies to the design of transmissive freeform surfaces. Luo [16,25] et al. first constructed a point light source model by separating variables, then modified the preset distribution according to the actual irradiance distribution, and finally established a new irradiance distribution by iterative function, thus completing the design of freeform mirror. A rectangular spot distribution with an irradiance uniformity of 81.08% was achieved by this method. Based on the existing freeform surface design ideas, we propose a new discretization method for the initial structure of the freeform surface, based on the definition of Chebyshev points, a two-dimensional extension is carried out to make it a better match between the projection grid of the light emitted from the light source, to improve the continuity of the surface and the uniformity of the reflected light. In the next section, we introduce the method of establishing and solving the freeform surface mathematical model.

3. Freeform reflector design principle

3.1. Establishment of the mathematical model

The essence of the design and solving method proposed in this section is to transfer the energy from the light source to the target plane in a reasonable way by a freeform reflector. As shown in Fig. 2 is the diagram of energy transfer for a freeform reflector. According to the law of conservation of energy, the energy received by the target surface is equal to the energy of the light source incident on the freeform reflector multiplied by the reflectance of the reflector. Then the Jacobi matrix can be used to achieve the energy conversion between each face. As long as the

Optics EXPRESS

irradiance in each illumination area unit is equal, an irradiance uniformity spot can be obtained on the target plane.

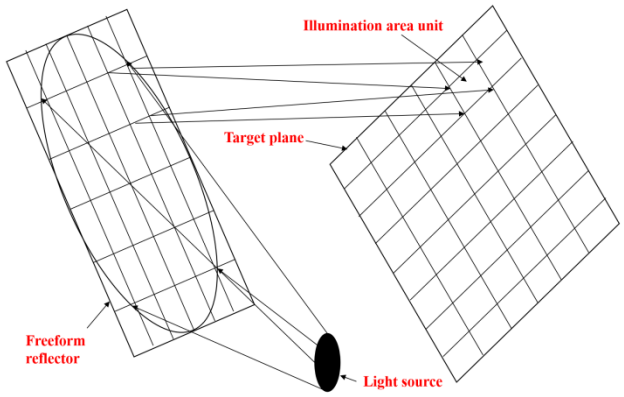

Fig. 2. Diagram of energy transfer for a freeform reflector.

As shown in Fig. 3(a) is the 3D diagram of the illumination coordinate system, Fig. 3(b) is the corresponding 2D diagram. According to the design and solving method, first, a spherical coordinate system with a radius of 1 is constructed. All subsequent variables are normalized to facilitate calculation. Assuming that the surface type region of the freeform reflector is Ω_0, and the projection region of the luminous region emitted by the light source on the unit sphere is $\rho(u, v)$, where ρ is the distance between the light source and the freeform reflector, and the region of reflection projection on the target surface is Ω_1. The Ω_0, Ω_1 and point O have been marked in Fig. 1. The topological plane $u_1 - v_1$ is titled β from plane $u - v$. The target surface $t_x - t_y$ is shifted upward 2 units form plane $u - v$; $t_x - t_y$ is called the target plane of the incident area of the light source. The purpose is to convert the irregular region of incident light on the unit sphere into a plane to facilitate calculation.

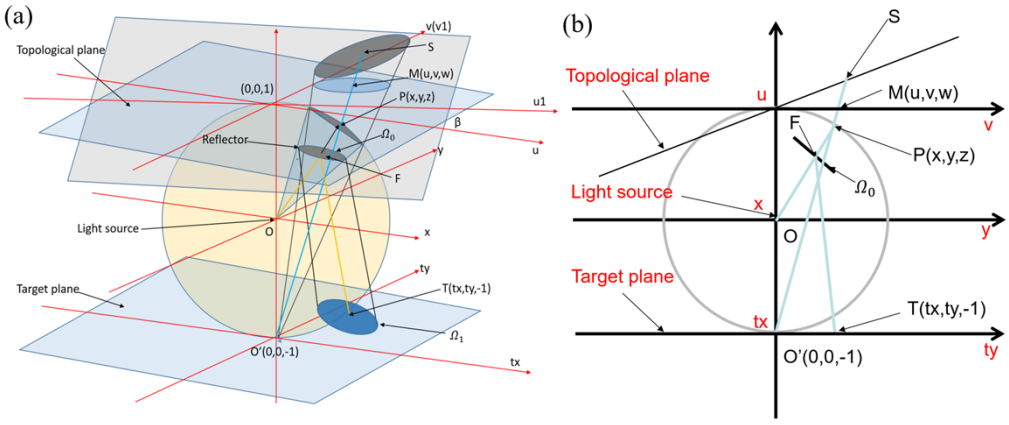

Fig. 3. Diagram of the illumination coordinate system: (a) 3D (b) 2D.

Assuming that the intensity of the input light source OP is I, M is the projection of point P on the plane z = 1 along the line through the south pole (0, 0, -1) of the unit sphere and point P. With coordinates u and v, M can be expressed as I(u,v). We assume that there is no energy loss in the

Optics EXPRESS

optical system during the design stage. According to the law of conservation of energy, we have:

$$\iint_{\Omega_1} E(t_x, t_y)dt_x dt_y = \iint_{\Omega} I(u, v)d\Omega. \tag{1}$$

where E is the irradiance of a point at the coordinate (t_x, t_y), Ω_1 is the illumination area on the target plane which can also be regarded as the diffuser as shown in Fig. 1, and Ω is the solid angle of the output light. Assuming that plane $u_1 - v_1$ is titled along the x-axis, and the obtained point in plane $u_1 - v_1$ is $S(u_1, v_1, 0)$, as the plane $u_1 - v_1$ is titled β from the plane u − v, then point S in the coordinate u − vcan be expressed as:

$$\begin{bmatrix} u \\ v \\ w \end{bmatrix} = \begin{bmatrix} 1 & 0 & 0 \\ 0 & \cos\beta & \sin\beta \\ 0 & -\sin\beta & \cos\beta \end{bmatrix} \begin{bmatrix} u_1 \\ v_1 \\ 0 \end{bmatrix}. \tag{2}$$

By solving Eq. (2), we can obtain point S in the coordinate u − v is $(u_1, v_1\cos\beta, -v_1\sin\beta)$.

As the plane is shifted upward 1 unit from the plane, the coordinate of point S in the coordinate x − y is $(u_1, v_1\cos\beta, 1 - v_1\sin\beta)$. At this point, the equation of the line O′SP can be expressed as:

$$\frac{x}{u_1} = \frac{y}{v_1\cos\beta} = \frac{z+1}{2 - v_1\sin\beta} = k. \tag{3}$$

Since point P is on the sphere, it needs to satisfy the following equation:

$$x^2 + y^2 + z^2 = 1. \tag{4}$$

Solving Eqs. (3) and (4),

$$k = \frac{2(2 - v_1\sin\beta)}{u_1^2 + v_1^2 - 4v_1\sin\beta + 4}. \tag{5}$$

The vector of the output light ray is **OP**, considering the points S (u, v, 1) and P (x, y, z). Defining **OP** to be the vector **m**, it can then be expressed as

$$\mathbf{m}(u_1, v_1) = \frac{1}{u_1^2 + v_1^2 - 4v_1\sin\beta + 4} \begin{pmatrix} 2u_1(2 - v_1\sin\beta), \\ 2v_1\cos\beta(2 - v_1\sin\beta), \\ (2 - v_1\sin\beta)^2 - v_1^2\cos^2\beta - u_1^2 \end{pmatrix}. \tag{6}$$

As the energy of the output light is contained within the solid angle, we obtain

$$d\Omega = |\mathbf{m_{u_1}} \times (\mathbf{m_{v_1}}\cos\beta)|du_1 dv_1. \tag{7}$$

where $\mathbf{m_{u1}}$ and $\mathbf{m_{v1}}$are the partial derivatives of **m** with respect to u and v, respectively. $\mathbf{m_{u1}}$ and $\mathbf{m_{v1}}$ can be expressed as

$$\begin{aligned} \mathbf{m_{u1}} = [&-\frac{4{u_1}^2(2 - v_1\sin\beta)}{(4 + {u_1}^2 + {v_1}^2 - 4v_1\sin\beta)^2} + \frac{2(2 - v_1\sin\beta)}{4 + {u_1}^2 + {v_1}^2 - 4v_1\sin\beta}, \\ &-\frac{4u_1v_1\cos\beta(2 - v_1\sin\beta)}{(4 + {u_1}^2 + {v_1}^2 - 4v_1\sin\beta)^2}, \\ &-\frac{2u_1}{4 + {u_1}^2 + {v_1}^2 - 4v_1\sin\beta} - \frac{2u_1(-{u_1}^2 - {v_1}^2\cos^2\beta + (2 - v_1\sin\beta)^2)}{(4 + {u_1}^2 + {v_1}^2 - 4v_1\sin\beta)^2}]. \end{aligned} \tag{8}$$

Optics EXPRESS

$$\mathbf{m_{v_1}} = [-\frac{4u_1(v_1 - 2\sin\beta)(2 - v_1\sin\beta)}{(4 + {u_1}^2 + {v_1}^2 - 4v_1\sin\beta)^2} - \frac{2u_1\sin\beta}{4 + {u_1}^2 + {v_1}^2 - 4v_1\sin\beta},$$
$$-\frac{4v_1\cos\beta(v_1 - 2\sin\beta)(2 - v_1\sin\beta)}{(4 + {u_1}^2 + {v_1}^2 - 4v_1\sin\beta)^2} + \frac{4\cos\beta(1 - v_1\sin\beta)}{4 + {u_1}^2 + {v_1}^2 - 4v_1\sin\beta}, \quad (9)$$
$$-\frac{2v_1\cos^2\beta + 2\sin\beta(2 - v_1\sin\beta)}{4 + {u_1}^2 + {v_1}^2 - 4v_1\sin\beta} - \frac{2(v_1 - 2\sin\beta)(-{u_1}^2 - {v_1}^2\cos^2\beta + (2 - v_1\sin\beta)^2)}{(4 + {u_1}^2 + {v_1}^2 - 4v_1\sin\beta)^2}].$$

using Eqs. (8) and (9), Eq. (7) then becomes

$$d\Omega = \frac{8\cos^2\beta|-2 + v_1\sin\beta|}{(4 + {u_1}^2 + {v_1}^2 - 4v_1\sin\beta)^2}du_1dv_1. \quad (10)$$

when $\beta = 0$,

$$d\Omega = (1 + 0.25w^2)^{-2}dudv. \quad (11)$$

where $w^2 = u^2 + v^2$. The directions of vectors **OF** and **OP** are aligned, and **OP** is the unit vector. If the distance between the source position O and the point F is ρ, the vector **OF** can be expressed as:

$$\mathbf{A} = \rho\mathbf{m} = \rho(\frac{u}{1 + 0.25w^2}, \frac{v}{1 + 0.25w^2}, \frac{1 - 0.25w^2}{1 + 0.25w^2}). \quad (12)$$

According to the law of reflection, the relationship between vectors **A** and **T** is shown in Fig. 4, **T** represents the vector **OT**; vector **A** of the emergent ray and the unit normal vector **N** at point F can be expressed as:

$$\frac{\mathbf{A}}{|\mathbf{A}|} + \frac{\mathbf{A} - \mathbf{T}}{|\mathbf{T} - \mathbf{A}|} = \frac{2\mathbf{N}(\mathbf{A}\cdot\mathbf{N})}{|\mathbf{A}||\mathbf{N}|^2}. \quad (13)$$

and

$$\mathbf{N} = \mathbf{A_u} \times \mathbf{A_v} = (\rho_u\mathbf{m} + \rho\mathbf{m_u}) \times (\rho_v\mathbf{m} + \rho\mathbf{m_v})$$
$$= \rho^2(1 + 0.25w^2)^{-2}\mathbf{m} - \rho_u\rho\mathbf{m_u} - \rho_v\rho\mathbf{m_v}. \quad (14)$$

where $\mathbf{A_u}$ and $\mathbf{A_v}$are the partial derivatives of **A** with respect to u and v, respectively, $\rho_\mathbf{u}$ and $\rho_\mathbf{v}$ are the partial derivatives of ρ with respect to u and v, respectively, and **F** and **G** can be defined as follows:

$$\mathbf{F} = |\mathbf{T} - \mathbf{A}|(1 + 0.25w^2)^{-1}$$
$$[\rho^2(1 + 0.25w^2)^{-2} + {\rho_u}^2 + {\rho_v}^2]^{-1}. \quad (15)$$

$$\mathbf{G} = (1 + 0.25w^2)^{-1} + \mathbf{F}[-\rho^2(1 + 0.25w^2)^{-2}$$
$$+ {\rho_u}^2 + {\rho_v}^2 - \rho(\rho_u u + \rho_v v)(1 + 0.25w^2)^{-1}]. \quad (16)$$

Finally, the coordinates of point T can be calculated as follows:

$$t_x = u\mathbf{G} + 2\rho_u\rho_v\mathbf{F}, t_y = v\mathbf{G} + 2\rho_u\rho_v\mathbf{F}. \quad (17)$$

This equation can be rewritten as:

$$t_x = t_x(u, v, \rho, \rho_u, \rho_v),\ t_y = t_y(u, v, \rho, \rho_u, \rho_v). \quad (18)$$

Based on the law of energy conservation, the relationship between the total energy of the outgoing light and the total energy of the target surface irradiation region can be obtained as

Optics EXPRESS

follows:

$$\iint_{\Omega_1} E(t_x, t_y)dt_x dt_y = \iint_{\Omega} I(u, v)d\Omega. \tag{19}$$

where Ω is the solid angle of the outgoing light. According to the mathematical model established by Schruben,

$$dt_x dt_y = |J(T)|dudv, |J(T)| = \begin{vmatrix} \frac{\partial t_x}{\partial u} & \frac{\partial t_x}{\partial v} \\ \frac{\partial t_y}{\partial u} & \frac{\partial t_y}{\partial v} \end{vmatrix}. \tag{20}$$

Then Eq. (19) can be rewritten:

$$E(t_x, t_y)\begin{vmatrix} \frac{\partial t_x}{\partial u} & \frac{\partial t_x}{\partial v} \\ \frac{\partial t_y}{\partial u} & \frac{\partial t_y}{\partial v} \end{vmatrix} dt_x dt_y = I(u, v)(1 + 0.25w^{2^{-2}})dt_x dt_y. \tag{21}$$

Based on the optimal transmission theory, the MA equation of the system can be obtained as follows:

$$a_1(\rho_{uu}\rho_{vv} - \rho_{uv}^2) + a_2\rho_{uu} + a_3\rho_{uv} + a_4\rho_{vv} + a_5 = 0. \tag{22}$$

$$\begin{aligned}
a_1 &= \frac{\partial t_x}{\rho_u}\frac{\partial t_y}{\rho_v} - \frac{\partial t_x}{\rho_u}\frac{\partial t_y}{\rho_v} \\
a_2 &= \frac{\partial t_x}{\rho_u}\frac{\partial t_y}{v} - \frac{\partial t_x}{v}\frac{\partial t_y}{\rho_u} + \rho_v\left(\frac{\partial t_x}{\rho_u}\frac{\partial t_y}{\rho} - \frac{\partial t_x}{\rho}\frac{\partial t_y}{\rho_u}\right) \\
a_3 &= \frac{\partial t_x}{\rho_v}\frac{\partial t_y}{v} - \frac{\partial t_x}{v}\frac{\partial t_y}{\rho_v} + \frac{\partial t_x}{u}\frac{\partial t_y}{\rho_u} - \frac{\partial t_x}{\rho_u}\frac{\partial t_y}{u} + \rho_u\left(\frac{\partial t_x}{\rho}\frac{\partial t_y}{\rho_u} - \frac{\partial t_x}{\rho_u}\frac{\partial t_y}{\rho}\right) + \rho_v\left(\frac{\partial t_x}{\rho_v}\frac{\partial t_y}{\rho} - \frac{\partial t_x}{\rho}\frac{\partial t_y}{\rho_v}\right) \\
a_4 &= \frac{\partial t_x}{u}\frac{\partial t_y}{\rho_v} - \frac{\partial t_x}{\rho_v}\frac{\partial t_y}{u} + \rho_u\left(\frac{\partial t_x}{\rho}\frac{\partial t_y}{\rho_v} - \frac{\partial t_x}{\rho_v}\frac{\partial t_y}{\rho}\right) \\
a_5 &= \frac{\partial t_x}{u}\frac{\partial t_y}{v} - \frac{\partial t_x}{v}\frac{\partial t_y}{u} + \rho_u\left(\frac{\partial t_x}{\rho}\frac{\partial t_y}{v} - \frac{\partial t_x}{v}\frac{\partial t_y}{\rho}\right) + \rho_u\left(\frac{\partial t_x}{u}\frac{\partial t_y}{\rho} - \frac{\partial t_x}{\rho}\frac{\partial t_y}{u}\right).
\end{aligned} \tag{23}$$

where $\rho_{\mathbf{uu}}$ and $\rho_{\mathbf{vv}}$are the second partial derivative of ρ with respect to u and v, respectively, $\rho_{\mathbf{uv}}$ is the mixed partial derivative of ρ with respect to u and v. Thus, the mathematical model is completed.

$$\begin{cases} a_1(\rho_{uu}\rho_{vv} - \rho_{uv}^2) + a_2\rho_{uu} + a_3\rho_{uv} + a_4\rho_{vv} + a_5 = 0 \\ \text{BC}: \begin{cases} t_x = t_x(u, v, \rho, \rho_u, \rho_v) \\ t_y = t_y(u, v, \rho, \rho_u, \rho_v) \end{cases} : \quad \partial\Omega_0 \rightarrow \partial\Omega_1 \ . \end{cases} \tag{24}$$

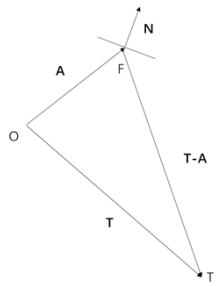

Fig. 4. .Law of reflection.

Optics EXPRESS

3.2. Chebyshev point and Chebyshev grid

In a freeform reflector illumination system, when the light source has rotational symmetry, the projection area of the light source is circular, whereas the sampling grid is usually topological squares or rectangles [26,27]; this results in a mismatch between the two. Therefore, in this paper, the method of discretization of the circular region is proposed. The specific implementation methods are as follows: 1) The system is designed by using the mapping from target irradiation to light source emission; 2) The boundary condition is the mapping between the boundary of the irradiation output region and the boundary of the light source emission region; 3) Select the luminous region of the light source, and set its projection boundary to match the mapping boundary. On this basis, the solution of the mathematical model of the optical system is obtained, and the problem of mismatch between the projected area of the light source and the sampling grid is solved. When the area of the mirror is large, 41×41 or 81×81 points can be used as the discretization condition, as shown in Fig. 5.

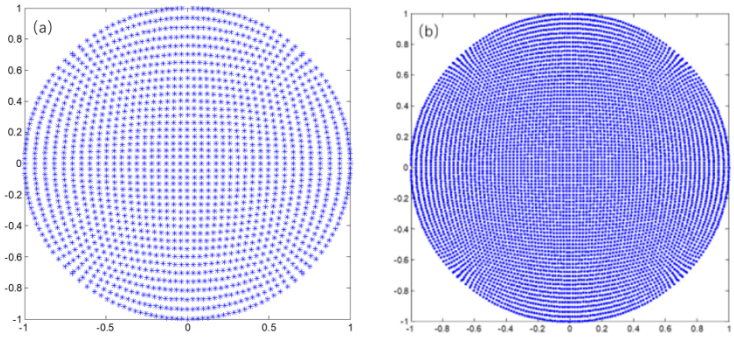

Fig. 5. Chebyshev points on freeform reflector: (a) 41×41 points (b) 81×81 points.

Here, only a numerical solution can be used; hence, it is impossible to obtain an accurate answer. First, we must discretize the elliptic Monge-Ampère equation and the nonlinear boundary condition [28]. $h_i = \rho_{i+1,j} - \rho_{i,j}$ and $h_j = \rho_{i,j+1} - \rho_{i,j}$ are the spacings in u- and v-axes, respectively, as shown in Fig. 6. The grid points along Ω_0 are called the boundary points, and the grid points inside Ω_0 are the interior points. Therefore, each interior point should satisfy the elliptic Monge-Ampère equation, and each boundary point should satisfy the boundary condition. Subsequently, we use the difference formula for derivatives to discretize the elliptic Monge-Ampère equation and the nonlinear boundary condition.

For the interior point, we define the scheme shown in Fig. 6 as:

$$\begin{aligned}\rho_u &= \frac{\rho_{i+1,j}-\rho_{i-1,j}}{2h_i},\rho_v = \frac{\rho_{i,j+1}-\rho_{i,j-1}}{2h_j},\rho_{uu} = \frac{\rho_{i+1,j}-\rho z_{i,j}+\rho_{i-1,j}}{h_i^2}\\ \rho_{vv} &= \frac{\rho_{i,j+1}-2\rho_{i,j}+\rho_{i,j-1}}{h_j^2},\rho_{uv} = \frac{\rho_{i+1,j+1}-\rho_{i+1,j-1}-\rho_{i-1,j+1}+\rho_{i-1,j-1}}{4h_ih_j}.\end{aligned} \tag{25}$$

Taking $u = u_{max}$ as an example of the boundary line, as shown in Fig. 6, by one-sided finite differences, we find that:

$$\rho_u = \frac{3\rho_{m,j}-4\rho_{m-1,j}+\rho_{m-2,j}}{2h_i},\rho_v = \frac{\rho_{m,j+1}-\rho_{m,j-1}}{2h_j}. \tag{26}$$

Equation (22) can be rewritten in $(m+1)(n+1)$ equation sets and there are $(m+1)(n+1)$ Chebyshev points. The intensity of the point source obeys the lambert characteristic, the

Optics EXPRESS

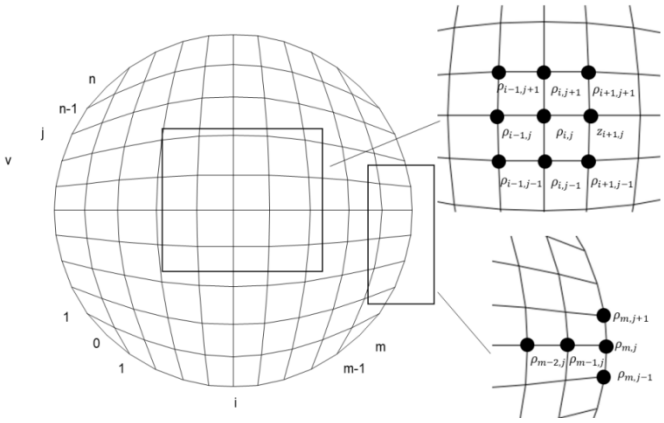

Fig. 6. Nine-point finite difference scheme for the interior points and boundary points.

intensity $I(u, v)(1 + 0.25w^2)^{-2}$can then be obtained. Solving the $(m + 1)$ $(n + 1)$ equation sets, the coordinates of the points on the freeform reflector can be determined. Newton downhill method is used to solve all the remaining points. Finally, the freeform surface can be constructed, and the Bezier surface pieces proposed by Wu et al. [29] are used to suture each piece to obtain the final freeform surface model.

4. Simulation and testing

4.1. Off-axis reflected illumination model

Based on the freeform surface model establishment and solution method proposed in the previous section, we designed the SCAR-based radiation calibration system freeform reflector in detail. The design process is shown in Fig. 7.

The structural parameters of each part of the radiometric calibration light source system are shown in Table 1.

Table 1. Design parameters of the freeform reflector.

Parameters	value
θ/°	15
β/°	22.5
γ/°	45
r/mm	400
z/mm	900
F#	1.6

Here θ is the luminous angle of the light source, β is the deflection angle of the freeform reflector, γ is the tilt angle of the diffuser, r is the distance between the light source and the freeform reflector, Z is the distance between the target surface and the freeform reflector, and $F\#$ is the F-number of the system, which is represented by the ratio of the distance between the reflector and the light source and the maximum aperture of the reflector. The discrete point data are obtained by solving using MATLAB. At this time, the discrete graph model of the freeform reflector is obtained by using Chebyshev points, as shown in Fig. 8; 81×81 points are used. Equation (5) is solved to obtain the freeform reflector model, as shown in Fig. 9.

Optics EXPRESS

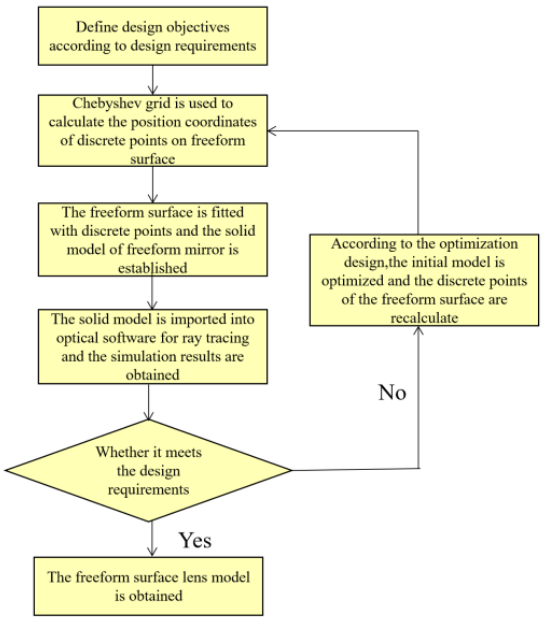

Fig. 7. Design flowchart.

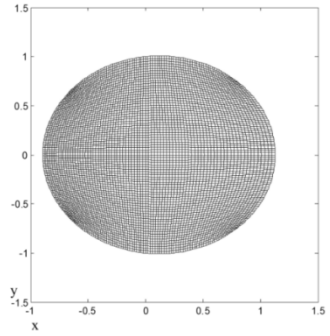

Fig. 8. Schematic of Chebyshev points.

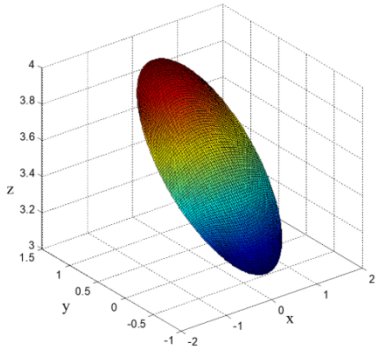

Fig. 9. Schematic of the freeform reflector simulation.

Optics EXPRESS

The results are imported into the LightTools optical software. The optical simulation is carried out according to the optical path of the whole spectral calibration light source, the schematic of the illumination is shown in Fig. 10. It is worth noting that the previous derivations are based on point light source, but the light source in Fig. 10 is a circular outlet with a diameter of 22 mm of a small integrating sphere. If an extended light source is used to replace the point light source, the irradiance of the boundary region on the target surface will show a large trapezoidal decline, as shown in Fig. 11(a). Therefore, the freeform reflector solved based on the point source model cannot be directly applied to the actual calibration task. Here we apply a feedback optimization method which we have used before to optimize the freeform reflector. The feasibility of this method has been demonstrated previously in coaxial systems [30].

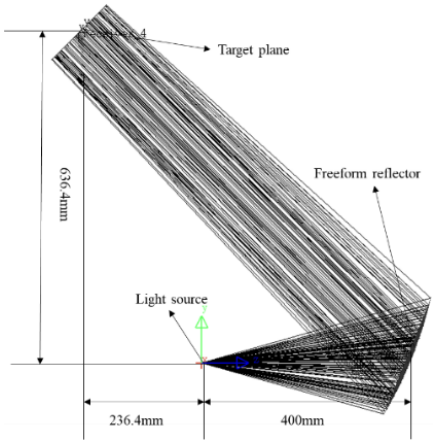

Fig. 10. The model of light path.

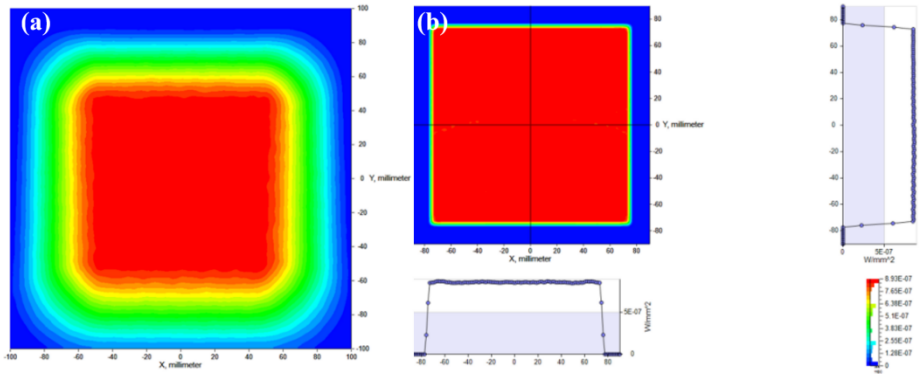

Fig. 11. A square illuminated area with a side length of 150 mm: (a) before optimization (b) after optimization.

The irradiance simulation result of the target plane after optimized is shown in Fig. 11(b), it can be seen that the illumination area formed by the freeform reflector on the target plane is larger than 120 mm × 120 mm which is sufficient to cover the diffuser and is of good uniformity. The simulation results show that the freeform reflector design method based on Chebyshev points can achieve ideal uniformity and illumination area, and it is feasible to be applied to turn and collimate the optical path in the SCAR-based radiation calibration system. To verify this result, detailed tests on the freeform reflector and calibration light source system were conducted.

Optics EXPRESS

4.2. Actual test

According to the above freeform reflector simulation model established based on the off-axis reflection illumination model of the SCAR-based radiation calibration system, the freeform reflector structure model was constructed as shown in Fig. 12(a). The surface of the model is smooth and continuous, which results in good machinability. Moore Nanotech 250UPL precision single-point diamond machining machine was used to process the freeform reflector, and the real object is shown in Fig. 12(b). The whole freeform reflector is made of aluminum. In order not to damage the surface of the reflector, the surface is not coated. And then a series of tests were conducted on the roughness of the freeform reflector and the optical properties of the freeform calibration light source system.

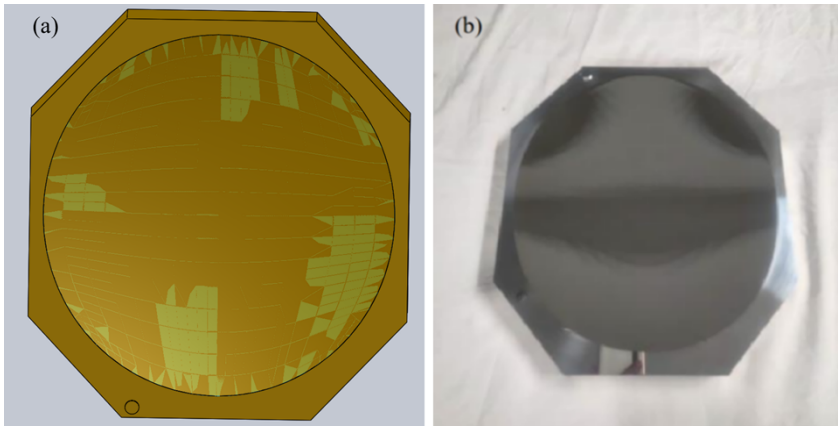

Fig. 12. (a) Freeform reflector model pattern, (b) freeform reflector physical pattern.

LUPHO Scan scanner was used to detect the surface shape of the freeform reflector and obtained the roughness data. The test results are shown in Fig. 13, where the RMS is 0.61 μm. The test results show that the processed freeform reflector has no obvious tool marks and the continuity of the processed surface is good, which can meet the practical application.

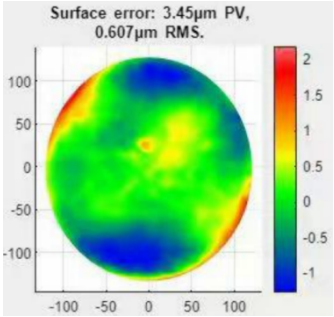

Fig. 13. Test results of surface roughness of the freeform reflector.

As shown in Fig. 14, the freeform reflector was integrated into the SCAR-based radiation calibration system for light path bending and collimation. As expected before, after the bending and collimation of the freeform reflector, a light spot is formed on the diffuser, which is sufficient to cover the 120 mm × 120 mm diffuser. The uniformity of the spot will be evaluated by experimental tests.

Optics EXPRESS

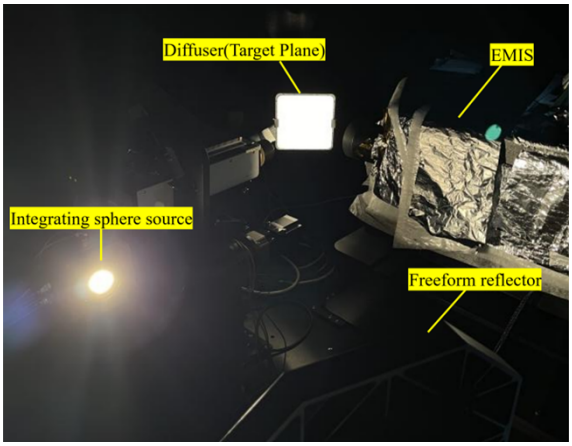

Fig. 14. Uniform whole spectral calibration light source.

As mentioned before, the size of the light spot created by the freeform reflector on the diffuser needs to be large enough because the diffuser needs to cover the observation area of EMIS and TR, and the irradiance uniformity of the light spot at the diffuser position (Target Plane) is supposed to be better than 98% in the 100 mm × 100 mm region. The location of the target plane is shown in Fig. 15. In this regard, the spot size and its uniformity were tested in detail.

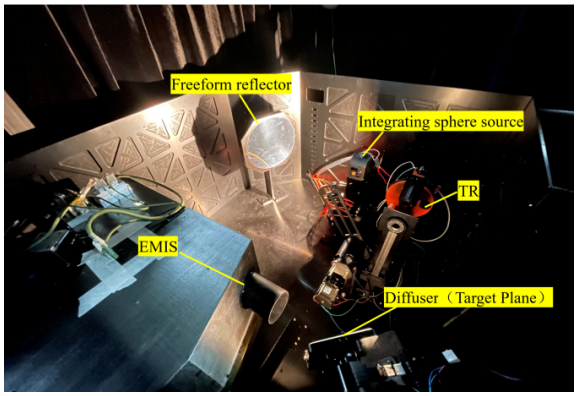

Fig. 15. The location of the target plane.

The grid-scanning method is used to detect the light spot formed by the freeform reflector on the target plane, and the scheme is shown in Fig. 16. We fixed the Hamamatsu S2281 Si-photodiode on a electric two-dimensional guide rail, and placed the two-dimensional guide rail on the position of the diffuser to drive S2281 to perform point-by-point scanning in the target plane, this is used to measure the irradiance in each small area received by the diffuser. After connecting the detector to an amplification box and a calibrated 6½ digit digital multimeter, three groups of data were measured at each measuring point and the average value was taken as the irradiance data at that point. The scan area is 150 mm × 150 mm, and the scan step is 10 mm.

Denote the relative position of the test point to the center of the diffuser in two directions by X and Y, respectively. The normalized test result of irradiance is shown in Fig. 17. It can be seen from the data that due to the smoothness and continuity of the freeform reflector, the irradiance distribution of its reflected light on the target plane is also continuous without obvious

Optics EXPRESS

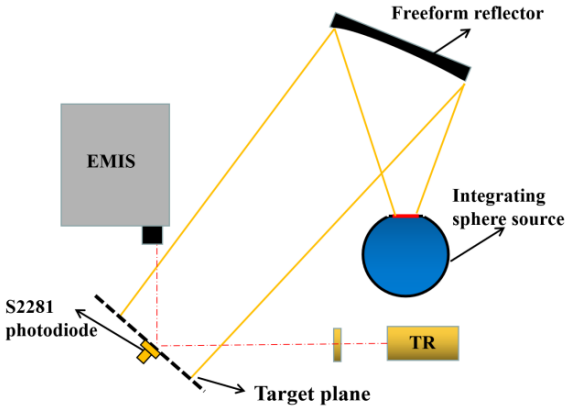

Fig. 16. Irradiance uniformity test scheme.

mutation point. The diameter of the photosensitive surface of S2281 is 11.3 mm, so a 10×10 scanning grid can cover the test area of 100 mm $\times$ 100 mm. As shown in Table 2, we extracted 10×10 data points in the center of the scanned grid for analysis, Eq. (27) is used to calculate the irradiance nonuniformity u, where E_{max} is the maximum irradiance value and E_{min} is the minimum irradiance value in grid data. After calculation, the irradiance uniformity in the test area is 98.2%, which meets the requirement of uniformity better than 98%.

$$u = \frac{E_{max} - E_{min}}{E_{max} + E_{min}} \tag{27}$$

In addition, to verify the radiance uniformity of the freeform calibration light source system, we use SVC HR1024i spectrometer to measure the radiance in the way of grid scanning, the test diagram is shown in Fig. 18. The SVC was placed in the same observation direction as the EMIS, and was driven by a two-dimensional guide rail for point-by-point scanning. The diameter of the SVC observation area on the diffuser is about 45 mm, so a 5 by 5 grid test with a step size of 15 mm is sufficient to cover the 100 mm $\times$ 100 mm illuminated area.

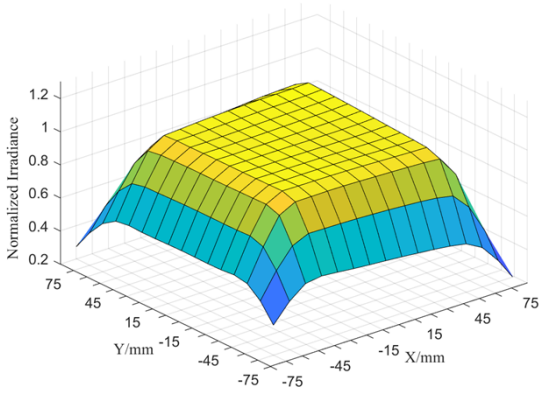

Fig. 17. Normalized test data for irradiance uniformity.

The test data of two spectral channels were selected of SVC for uniformity analysis. As shown in Fig. 19(a) and Fig. 19(b) is normalized radiance test data at 1036.9 nm and 780.8 nm, respectively. Equation (27) was also used to evaluate the uniformity of grid test data. After calculation,

Optics EXPRESS

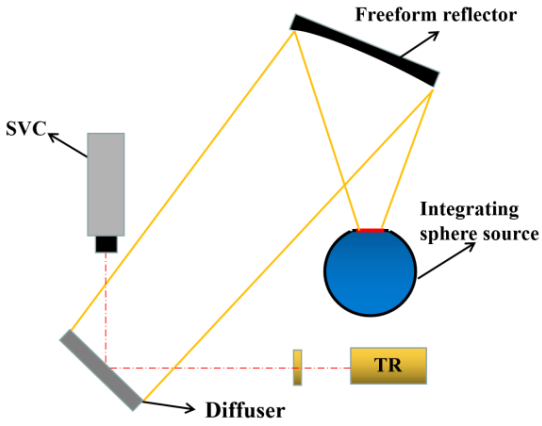

Fig. 18. Radiance uniformity test scheme.

Table 2. Normalized test data for irradiance.

Y\X	-45mm	-35mm	-25mm	-15mm	-5mm	+5mm	+15mm	+25mm	+35mm	+45mm
-45mm	0.9962	0.9981	0.9985	0.9995	1.0017	1.0046	1.0083	1.0125	1.0164	1.0193
-35mm	0.9981	0.9997	0.9995	1.0003	1.0018	1.0043	1.0077	1.0107	1.0128	1.0128
-25mm	0.9992	1.0004	1.0003	1.0010	1.0023	1.0042	1.0067	1.0087	1.0092	1.0070
-15mm	1.0001	1.0008	1.0008	1.0010	1.0019	1.0033	1.0047	1.0060	1.0052	1.0019
-5mm	1.0006	1.0013	1.0009	1.0010	1.0015	1.0027	1.0023	1.0026	1.0009	0.9963
+5mm	1.0011	1.0022	1.0015	1.0009	1.0004	1.0000	0.9989	0.9982	0.9962	0.9913
+15mm	1.0020	1.0032	1.0020	1.0006	0.9991	0.9971	0.9952	0.9941	0.9918	0.9872
+25mm	1.0037	1.0041	1.0017	0.9992	0.9967	0.9943	0.9922	0.9904	0.9877	0.9827
+35mm	1.0034	1.0019	0.9985	0.9953	0.9923	0.9894	0.9874	0.9861	0.9841	0.9816
+45mm	1.0096	1.0033	0.9963	0.9910	0.9874	0.9841	0.9818	0.9811	0.9819	0.9824

the uniformity of 1036.9 nm and 780.8 nm are both 98.5%, which meets the requirement of uniformity better than 2%.

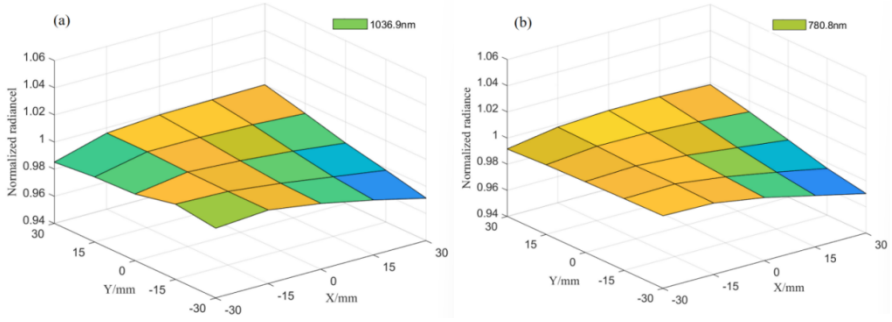

Fig. 19. Normalized test data for radiance: (a) 1036.9 nm (b) 780.8 nm.

Optics EXPRESS

5. Discussion

At present, the radiometric calibration of space remote sensing is faced with difficult problems such as poor consistency, poor data comparability of different remote sensors, and low radiometric calibration accuracy, this has greatly affected our monitoring and forecasting of the Earth's climate and environmental changes. The SCAR-based onboard radiation calibration system can greatly improve the credibility of space remote sensing data in both temporal and spatial dimensions. However, the load, space, and energy consumption of the calibration system are the factors that restrict its final performance on board. A freeform reflector can precisely control the light to reach a specified area, this can not only make the space layout of the whole calibration system more flexible and increase the space utilization but also improve the energy utilization and reduce the energy consumption. Most importantly, it can provide a large area of uniform light source for the calibration system, reduce the error introduced by the radiation transfer link, and improve the accuracy of the onboard calibration. Therefore, compared with the current illumination scheme, the onboard illumination mode based on the freeform reflector adopted in this paper more perfectly meets the requirements of onboard calibration in terms of both space, energy utilization and uniform light source. The freeform reflector light source has the potential to be used in more onboard calibration systems.

The Chebyshev spectrum method can be used for differential equations with boundary conditions and computation intervals showing non-periodicity. The initial structure discretization design method of freeform surface based on Chebyshev points proposed in this paper, starting from Chebyshev's basic definition, it is extended and derived in two dimensions, so that it can better match the projection grid of the light source. The advantage of this method lies in that not only the emission region of the light source is effectively discretized, but also the partial differential equation is decomposed into the ordinary differential equation by this method, and the solution of complex (MA) Monge-Ampère equation is transformed into solving ordinary differential equations, this also makes the design of freeform mirror easier and more universal. The freeform reflectors established based on this idea are more smooth and more continuous. As the core device of the calibration light source system, it provides important support for irradiance uniformity of reflected light.

6. Conclusion

This paper proposed a new onboard calibration light source system based on a freeform reflector for the SCAR-based radiation calibration system. A new design idea for the freeform surface is also put forward according to the present freeform surface design method. Based on the characteristics of Chebyshev meshes, the topological meshes of the outgoing light can be discretized inhomogeneous. At the same time, the freeform surface model with a good initial structure is directly generated by the Optimal mass Transport (OMT) theory. Finally, the Bessel curve is used to control and adjust the discrete points, and a continuous smooth freeform surface is constructed. The constructed freeform reflector is simulated and analyzed according to the light path of the SCAR-based radiation calibration system, the size and uniformity of the spot formed in the target plane can meet the application requirements. Then we processed the designed freeform reflector and tested its surface roughness, the result shows that the RMS is 0.61 μm and the continuity of the machining surface is good. We integrate it into the calibration system and use S2281 Si-photodiode and SVC spectrometer respectively to measure the irradiance of the effective illumination area in the target plane and the radiance of the diffuser with grid-scanning method. The experimental results show that in the effective illumination area of 100 mm × 100 mm of the target plane, the irradiance uniformity of the diffuser and the light emitted from the freeform reflector are 98.5% and 98.2%, respectively, which are both better than 98% and meet the practical application requirements. The designed freeform reflector can be perfectly applied

Optics EXPRESS

to the optical path bending and collimation of the SCAR-based radiation calibration system. The freeform reflector calibration light source system not only provides high uniformity calibration light source for onboard radiometric calibration, but also improves the space utilization of the calibration system, reduces on-board resource consumption, and also provides the possibility to achieve the goal of the spectral radiance measurement uncertainty better than 1% on the reflected solar band of Chinese Space-based Radiometric Benchmark (CSRB).

Funding. Strategic Priority Research Program of the Chinese Academy of Sciences (XDA28050103); National Key Research and Development Program of China (2018YFB0504600, 2018YFB0504603).

Acknowledgments. XinYe thanks Strategic Priority Research Program of the Chinese Academy of Sciences and National Key R&D Program of China under grant for help identifying collaborators for this work.

Disclosures. The authors declare no conflicts of interest.

Data availability. Data underlying the results presented in this paper are not publicly available at this time but may be obtained from the authors upon reasonable request.

References

1. J. Xiong, C. Cao, and G. Chander, "An overview of sensor calibration inter-comparison and applications," Front. Earth Sci. China **4**(2), 237–252 (2010).
2. X. Q. Hu, Y. X. Zhang, Z. Q. Liu, G. S. Zhang, Y. B. Huang, K. M. Qiu, Y. K. Wang, L. J. Zhang, X. B. Zhu, and Z. G. Rong, "Optical characteristics of China Radiometric Calibration Site for Remote Sensing Satellite Sensors (CRCSRSSS)," Proc. SPIE **4151**, 77–86 (2001).
3. Y. P. Wang, X. Q. Hu, H. R. Wang, X. Ye, and W. Fang, "Standard transfer chain for radiometric calibration of optical sensing instruments with traceability in solar reflective bands," Opt. Precis. Eng. **23**(7), 1807–1812 (2015).
4. P. Zhang, N. Lu, C. Li, L. Ding, and J. Schmetz, "Development of the Chinese space-based radiometric benchmark mission LIBRA," Remote Sens. **12**(14), 2179 (2020).
5. N. Fox, A. K. Weiss, W. Schmutz, K. Thome, D. Young, B. A. Wielichi, R. Winkler, and E. Woolliams, "Accurate radiometry from space: An essential tool for climate studies," Phil. Trans. R. Soc. A **369**(1953), 4028–4063 (2011).
6. W. Sun and C. Lukashin, "Modeling polarized solar radiation from the ocean - atmosphere system for CLARREO inter-calibration applications," Atmos. Chem. Phys. **13**(20), 10303–10324 (2013).
7. X. Ye, X. L. Yi, C. Lin, W. Fang, K. Wang, Z. W. Xia, Z. H. Ji, Y. Q. Zheng, D. Sun, and J. Quan, "Instrument Development: Chinese Radiometric Benchmark of Reflected Solar Band Based on Space Cryogenic Absolute Radiometer," Remote Sens. **12**(17), 2856 (2020).
8. X. Ye, X. L. Yi, W. Fang, K. Wang, Y. Luo, Z. W. Xia, and Y. P. Wang, "Design and Investigation of Absolute Radiance Calibration Primary Radiometer," IET Sci. Meas. Technol. **12**(8), 994–1000 (2018).
9. K. C. Lei, X. Ye, Z. W. Xia, N. Xu, S. Q. Li, Y. C. Zhang, Y. W. Wang, Z. W. Liu, and Z. G. Li, "Design of a Compact Transfer Radiometer for a Radiometric Benchmark Transfer Chain," Sensors **22**(18), 6795 (2022).
10. W. W. Pang, X. B. Zheng, J. J. Li, and X. S. Shi, "High Accuracy Calibration Technology of Remote Sensor Tracing to Cryogenic Radiometer," J. Atmos. Environ. Opt. **9**(2), 138 (2014).
11. B. Y. Li, J. W. Ren, Z. Wan, X. S. Li, and J. X. Sun, "Research of large aperture integrating sphere used in the radiative calibration for space remote sensor," J. Optoelectron. Laser **24**(3), 464–469 (2013).
12. L. Hanssen, "Integrating-sphere system and method for absolute measurement of transmittance, reflectance, and absorptance of specular samples," Appl. Opt. **40**(19), 3196–3204 (2001).
13. A. Rabl and J. M. Gordon, "Reflector design for illumination with extended sources: the basic solutions," Appl. Opt. **33**(25), 6012–6021 (1994).
14. P. Davies, "Edge-Ray Principle Of Non-imaging Optics," J. Opt. Soc. Am. A **11**(4), 1256–1259 (1994).
15. T. L. R. Davenport, T. A. Hougha, and W. J. Cassarlya, "Optimi-zation for illumination systems: the next level of design," Proc. SPIE **5456**, 81–90 (2004).
16. Y. Luo, Z. Feng, Y. Han, and H. Li, "Design of compact and smooth freeform optical system with uniform illuminance for LED source," Opt. Express **18**(9), 9055–9063 (2010).
17. J. Schruben, "Formulation of a reflector-design problem for a lighting fixture," J. Opt. Soc. Am. **62**(12), 1498–1501 (1972).
18. C. R. Prins, J. H. M. Ten Thije Boonkkamp, J. Van Roosmalen, L. W. Ijzerman, and W. T. Tukker, "A Monge-Ampère-Solver for freeform Reflector Design," SIAM J. Sci. Comput. **36**(3), B640–B660 (2014).
19. T. Yang, Y. Duan, D. Cheng, and Y. Wang, "Freeform imaging optical system design: theories, development and applications," Acta Opt. Sin. **41**(1), 0108001 (2021).
20. V. Oliker, "Geometric and variational methods in optical design of reflecting surfaces with prescribed illuminance properties," Proc. SPIE **5942**, 594207 (2005).
21. V. Oliker, "Optical design of freeform ywo-mirror beam-shaping system," J. Opt. Soc. Am. A **24**(12), 3741–3752 (2007).
22. R. M. Wu, S. Q. Chang, Z. R. Zheng, L. F. Zhao, and X. Liu, "Formulating the design of two freeform lens surfaces for point-like light sources," Opt. Lett. **43**(7), 1619–1622 (2018).

Optics EXPRESS

23. R. M. Wu and H. Hua, "Direct design of aspherical lenses for extended non-Lambertian sources in three-dimensional rotational geometry," Opt. Express **24**(2), 1017–1030 (2016).
24. R. M. Wu, L. Xu, P. Liu, Y. Q. Zhang, Z. R. Zheng, H. F. Li, and X. Liu, "Freeform illumination design: a nonlinear boundary problem for the elliptic Monge–Ampére equation," Opt. Lett. **38**(2), 229–231 (2013).
25. L. Wang, K. Y. Qian, and L. Yi, "Discontinuous free-form lens design for prescribed irradiance," Appl. Opt. **46**(18), 3716–3723 (2007).
26. X. Mao, H. Li, Y. Han, and Y. Luo, "Polar-grids based source-target mapping construction method for designing freeform illumination system for a lighting target with arbitrary shape," Opt. Express **23**(4), 4313–4328 (2015).
27. J. Chaves, *Introduction To Nonimaging Optics* (CRC press, 2008).
28. M. J. H. Anthonissen, L. B. Romijn, J. H. M. Ten Thije Boonkkamp, and W. L. IJzerman, "Unified mathematical framework for a class of fundamental freeform optical systems," Opt. Express **29**(20), 31650–31664 (2021).
29. R. M. Wu, Z. R. Zheng, H. F. Li, and X. Liu, "Constructing optical freeform surfaces using unit tangent vectors of feature data points," J. Opt. Soc. Am. A **28**(9), 1880–1888 (2011).
30. J. W. Tian, X. Ye, and W. Fang, "Freeform reflector design for uniform illumination in a space-based remote sensor calibration system," Appl. Opt. **61**(16), 4678–4686 (2022).